

PVP-stabilized tungsten oxide nanoparticles inhibit proliferation of NCTC L929 mouse fibroblasts *via* induction of intracellular oxidative stress

A. L. Popov¹, A. M. Ermakov¹, T. O. Shekunova^{2,4}, A. B. Shcherbakov³, O. N. Ermakova¹, O. S. Ivanova⁴,
N. R. Popova¹, A. Ye. Baranchikov⁴, V. K. Ivanov^{4,*}

¹Institute of Theoretical and Experimental Biophysics, Russian Academy of Sciences,
Pushchino, Moscow region, 142290, Russia

²Lomonosov Moscow State University, Moscow, 119991, Russia

³Zabolotny Institute of Microbiology and Virology, National Academy of Sciences of Ukraine,
Kyiv, D0368, Ukraine

⁴Kurnakov Institute of General and Inorganic Chemistry, Russian Academy of Sciences, Moscow, 119991, Russia
antonpopovleonid@gmail.com, ao_ermakovy@rambler.ru, taisia.shekunova@yandex.ru, carotene@igic.ras.ru,
beoluchi@yandex.ru, runetta05@mail.ru, nellipopovaran@gmail.com, a.baranchikov@yandex.ru, *van@igic.ras.ru

PACS 68.65.k, 81.20.n, 82.70.Dd, 82.50.Hp, 87.17.Ec

DOI 10.17586/2220-8054-2019-10-1-92-101

In this study, photochromic PVP-stabilized tungsten oxide nanoparticles (WO_{3-x} NPs) were shown to exhibit a dose-dependent cytotoxic effect on mouse fibroblasts *in vitro*. WO_{3-x} NPs reduce viability and proliferative activity of the cells *via* induction of intracellular oxidative stress leading to apoptosis and cell death. WO_{3-x} NPs modulate the mRNA expression of a wide range of genes responsible for oxidative stress and the cell redox-system.

Keywords: tungsten oxide nanoparticles, cytotoxicity, apoptosis, fibroblasts.

Received: 3 January 2019

Revised: 22 January 2019

1. Introduction

Metal oxide-based nanomaterials are widely used in biomedical applications as radioprotectors, radiosensitizers, photosensitizers, contrast agents, etc. One of the most promising X-ray contrast agents is nanocrystalline tungsten oxide (WO_{3-x}) [1–5]. In recent years, WO_{3-x} NPs have also been widely employed in antibacterial coatings or biosensors [6, 7]. Due to the specific physical and chemical properties of WO_{3-x} NPs, such as high surface energy and surface-to-volume ratio, quantum confinement effects and local plasmon resonance effects, they can be used in photothermal cancer therapy [8, 9]. Sharker *et al.* synthesized dopamine-conjugated hyaluronic acid-coated WO₃ nanoparticles (WO₃-HA) which demonstrated quite efficient photothermal conversion with time-dependent tumor-specific accumulation [10]. Zhou *et al.* used tungsten oxide nanorods for effective photothermal therapy and CT imaging of the tumor model *in vivo* [11]. Liu *et al.* used PEGylated WO_{3-x} nanoparticles as photothermal agents under near-IR laser irradiation (980 nm, 0.5 W·cm⁻²). Additionally, PEGylated WO_{3-x} nanoparticles were shown to be effective CT imaging contrast agent on a tumor-bearing mouse model [12]. Liu *et al.* used ultrasmall WO_{3-x}@ γ -poly-L-glutamic acid (WO_{3-x}@ γ -PGA) nanoparticles with good photoacoustic and photothermal properties for effective photothermal-enhanced chemodynamic therapy [13]. AbuMousa demonstrated enhancement of photocatalytic activity of nanostructured silver loaded tungsten oxide providing high anticancer efficiency under UV radiation [14].

The usage of tungsten oxide in advanced therapeutic compositions requires an in-depth systematic study of their cytotoxicity including detailed investigation of molecular mechanisms of WO_{3-x} NPs action on mammalian cells. Here, we analyzed the cytotoxicity of PVP-stabilized WO_{3-x} nanoparticles using the mouse fibroblasts NCTC L929 cell line and provided the first report on the molecular mechanisms of WO_{3-x} nanoparticles' cytotoxic action.

2. Materials and methods

2.1. Synthesis and characterization of tungsten oxide nanoparticles

Ultrasmall hydrated tungsten oxide nanoparticles were synthesized by hydrothermal processing of tungstic acid in the presence of polyvinylpyrrolidone (PVP K-30, average mol. wt. 40,000) acting as template, stabilizer and growth regulator. Tungstic acid was prepared by ion-exchange method using sodium tungstate (Na₂WO₄) solution and strongly acidic cation exchange resin (Amberlite®IR120). Briefly, ion exchange resin (in hydrogen form)

was swelled in water and loaded into the glass column (filling volume 200 ml). Then, 100 ml of 0.05 M sodium tungstate solution was passed through the column dropwise, 4 g of PVP was added to the obtained eluent; the solution was transferred to the flask and stirred for 4 h under reflux. During heating a clear sol of hydrated WO_{3-x} was formed, as shown by the appearance of UV-absorption band at 325 nm and Tyndall cone observation. For cytotoxicity study, WO_{3-x} sol was diluted to prepare 0.1 – 25.0 mg/ml colloid solutions.

Comprehensive analysis of WO_{3-x} nanoparticles was performed as described elsewhere [15].

2.2. Investigation of WO_{3-x} photochromic properties

To analyze the photochromic properties of the PVP-stabilized WO_{3-x} sol, it was subjected to UV exposure (BLX-E312 chamber) for 10 min: then the absorption spectra of the irradiated sol were analyzed using an OceanOptics QE65000 spectrometer for every 10 seconds during 10 min. After that, the sample was subjected to UV exposure for the second time. Such procedure (cycle) was repeated 10 times. The volume of the sol was 2 ml, the sol was diluted by 50 fold, *i.e.* the WO_{3-x} concentration was about 0.0006 M. The temperature of the cuvette compartment was maintained at 37 °C.

2.3. Cell culture

In vitro experiments were performed using a mouse fibroblast NTCT L929 cell line. The cells were cultivated in a DMEM/F12 (1:1) medium containing 10 % of fetal bovine serum (FBS), 50 $\mu\text{g}/\text{mL}$ of penicillin, 50 $\mu\text{g}/\text{mL}$ of streptomycin and 1 % of L-glutamine. The cells were cultivated at 37 °C in a humid atmosphere containing 95 % air and 5 % CO_2 . The cells were seeded with the density of 30,000 – 35,000 per cm^2 . Fetal bovine serum (FBS), penicillin, streptomycin, Dulbecco's Modified Eagle Medium (DMEM), F12 medium, L-glutamine, trypsin/versene solution were purchased from PanEco and Biosintez, Russia. Six hours after cells attachment, the medium was replaced by a medium containing different concentrations of WO_{3-x} NPs. In the control experiments, the cells were cultured without WO_{3-x} NPs.

2.4. MTT assay

Determination of mitochondrial and cytoplasmic dehydrogenase activity in living cells was performed using the MTT assay, which is based on the reduction of a colorless tetrazolium salt (3-citiation[4,5-dimethylthiazol-2-yl]-2,5-diphenyltetrazolium bromide, MTT). 24, 48 and 72 h after cell incubation with WO_{3-x} NPs a standard MTT assay was performed.

2.5. Analysis of proliferative activity

Cells were seeded in 24 well plates. After incubation for 6 hours, WO_{3-x} NPs were added to the cells at various concentrations (1 – 15 mg/ml). After 24, 48 and 72 hours cells were counted using Clone Select Imager (Molecular Device, USA).

2.6. Live/Dead viability assay

To evaluate the cytotoxic effects of the WO_{3-x} NPs, a Live/Dead Viability Kit (Invitrogen, Life Technologies) was used. Cells attached to the 96-well plate were processed according to the manufacturer's protocol, and visualized 25 minutes after adding the dye with an Axiovert 200 fluorescence-light microscope (Carl Zeiss, Germany) and recorded by a Canon A620 digital camera (Canon, USA). The green signal (SYTO 9 $\lambda = 485/498$ nm) characterized live cells and the red signal (propidium iodide $\lambda = 535/617$ nm) characterized dead cells. For each cell group, four fields in each well were examined.

2.7. PCR-RT

In order to extract mRNAs a kit with magnetic particles was used, according to the manufacturer's protocol (Sileks, Russia). Reverse transcription was performed by a Sileks kit (Russia) using oligodT primer according to the manufacturers protocol. The produced cDNAs served as a real-time PCR matrix. The amplification was performed on a CFX-96 amplifier (BioRad, USA) or an ABI 7500 Fast Real-Time PCR System (Applied Biosystems, USA). We determined the expression of 96 genes responsible for key cell processes (Table 1).

TABLE 1. Selected gene groups for PCR-RT analysis

Description	Symbol	Description	Symbol
glutathione peroxidase 1	<i>Gpx1</i>	interleukin 22	<i>Il22</i>
glutathione peroxidase 2	<i>Gpx2</i>	alsin Rho guanine nucleotide exchange factor	<i>Als2</i>
glutathione peroxidase 3	<i>Gpx3</i>	apolipoprotein E	<i>ApoE</i>
glutathione peroxidase 4	<i>Gpx4</i>	chemokine (C-C motif)	<i>Ccl5</i>
glutathione peroxidase 5	<i>Gpx5</i>	excision repair cross-complementing rodent repair deficiency complementation group 2	<i>Ercc2</i>
glutathione peroxidase 6	<i>Gpx6</i>	excision repair cross-complementing rodent repair deficiency, complementation group 6	<i>Ercc6</i>
glutathione peroxidase 7	<i>Gpx7</i>	ferritin heavy polypeptide 1	<i>Fth1</i>
glutathione S-transferase kappa 1	<i>Gstk1</i>	glutamate-cysteine ligase, catalytic subunit	<i>Gclc</i>
glutathione S-transferase, pi 1	<i>Gstp1</i>	glutamate-cysteine ligase, modifier subunit	<i>Gclm</i>
EH-domain containing 2	<i>Ehd2</i>	glutathione synthetase	<i>Gss</i>
peroxiredoxin 1	<i>Prdx1</i>	heme oxygenase 1	<i>Hmox1</i>
peroxiredoxin 2	<i>Prdx2</i>	heat shock protein 90 alpha (cytosolic), class B member 1	<i>Hspa1a</i>
peroxiredoxin 3	<i>Prdx3</i>	isocitrate dehydrogenase 1 (NADP+), soluble	<i>Idh1</i>
peroxiredoxin 4	<i>Prdx4</i>	keratin 1	<i>Krt1,</i>
peroxiredoxin 5	<i>Prdx5</i>	myeloperoxidase	<i>Mpo</i>
peroxiredoxin 6	<i>Prdx6</i>	NAD(P)H dehydrogenase, quinone 1	<i>Nqo1</i>
adenomatosis polyposis coli	<i>Apc</i>	Parkinson disease (autosomal recessive, early onset) 7	<i>Park7</i>
catalase	<i>Cat</i>	prion protein	<i>Prnp</i>
cathepsin B	<i>Ctsb</i>	proteasome (prosome, macropain) subunit, beta type 5	<i>Psmb5</i>
dual oxidase 1	<i>Duox1</i>	sequestosome 1	<i>Sqstm1</i>
eosinophil peroxidase	<i>Epx</i>	thioredoxin 1	<i>Txn1</i>
lactoperoxidase	<i>Lpo</i>	thioredoxin interacting protein	<i>Txnip</i>
myeloperoxidase	<i>Mpo</i>	uncoupling protein 3 (mitochondrial, proton carrier)	<i>Ucp3</i>
prostaglandin-endoperoxide synthase 1	<i>Ptgs1</i>	xeroderma pigmentosum, complementation group A	<i>Xpa</i>
prostaglandin-endoperoxide synthase 2	<i>Ptgs2</i>	ataxia telangiectasia and Rad3 related	<i>Atr</i>
recombination activating gene 2	<i>Rag2</i>	cytoglobin	<i>Cygb</i>

erine (or cysteine) peptidase inhibitor, clade B, member 1b	<i>Serp1b1b</i>	dynamilin 2	<i>Dnm2</i>
thyroid peroxidase	<i>Tpo</i>	Fanconi anemia, complementation group C	<i>Fancc</i>
albumin	<i>Alb</i>	intraflagellar transport 172	<i>Ift172</i>
glutathione reductase	<i>Gsr</i>	myoglobin	<i>Mb</i>
sulfiredoxin 1 homolog (S. cerevisiae)	<i>Srxn1</i>	neuroglobin	<i>Ngb</i>
thioredoxin reductase 1	<i>Txnrd1</i>	solute carrier family 38, member 1	<i>Slc38a1</i>
thioredoxin reductase 2	<i>Txnrd2</i>	vimentin	<i>Vim</i>
thioredoxin reductase 3	<i>Txnrd3</i>	beta-2 microglobulin	<i>B2m</i>
superoxide dismutase 1, soluble	<i>Sod1</i>	heat shock protein 90 alpha (cytosolic), class B member 1	<i>Hsp90ab1</i>
superoxide dismutase 3, extracellular	<i>Sod3</i>	actin, beta	<i>Actb</i>
superoxide dismutase 2, mitochondrial	<i>Sod2</i>	glyceraldehyde-3-phosphate dehydrogenase	<i>Gapdh</i>
copper chaperone for superoxide dismutase	<i>Ccs</i>	glucuronidase, beta	<i>Gusb</i>
cytochrome b-245, alpha polypeptide	<i>Cyba</i>	mVPA1	<i>mVPA1</i>
neutrophil cytosolic factor 1	<i>Ncf1</i>		
neutrophil cytosolic factor 2	<i>Ncf2</i>		
nitric oxide synthase 2, inducible	<i>Nos2</i>		
NADPH oxidase 1	<i>Nox1</i>		
NADPH oxidase 4	<i>Nox4</i>		
NADPH oxidase activator 1	<i>Noxa1</i>		
NADPH oxidase organizer 1	<i>Noxol1</i>		
RecQ protein-like 4	<i>Recql4</i>		
stearoyl-Coenzyme A desaturase 1	<i>Scd1</i>		
uncoupling protein 2 (mitochondrial, proton carrier)	<i>Ucp2</i>		
aldehyde oxidase 1	<i>Aox1</i>		
flavin containing monooxygenase 2	<i>Fmo2</i>		
interleukin 19	<i>Il19</i>		

The analyzed genes were selected from <http://www.sabiosciences.com> database for PCR profiling of different biological processes. The level of gene transcription was normalized by the levels of expression of housekeeping genes β -actin, *B2m* (beta-2 microglobulin), *Hsp90ab1* (heat shock protein 90 alpha (cytosolic), class B member 1), *gapdh* (glyceraldehyde-3-phosphate dehydrogenase) and *Gusb* (glucuronidase, beta). Each measurement was repeated twice (internal repetition) and averaged for 2 independent samples. The obtained expression data were analyzed using <http://www.sabiosciences.com> online services, mayday-2.14 software (Center for Bioinformatics Tubingen, Germany) and the Genesis software.

2.8. Statistical analysis

The experiments were conducted in 3 or 4 repetitions. Experimental results were compared with the control. Statistical analysis was performed using the methods of variation statistics. We determined the mean values and the standard deviation of the mean. The significance of the difference between the groups was determined by Student t-test. The obtained data were processed using GraphPad 6.0 and Microsoft Excel 2007 software.

3. Results and discussion

The synthesized WO_{3-x} sol possesses good photochromic properties – it turns blue under UV radiation, and in the absence of the UV light it gradually becomes colorless. A detailed study of the sol's photochromic properties regeneration showed the changes in the sol's discolouration rate during the repeated UV exposure. Thus, after the first irradiation (cycle 1), the sol become almost completely colorless in 10 min (Fig. 1(a)). In turn, after the fifth and tenth irradiation (cycles 5 and 10, respectively) the sol remained light blue (Fig. 1(b,c)). It is also worth noting that the absorption coefficient of the WO_{3-x} sol after each irradiation cycle changed. To determine the possible influence of polyvinylpyrrolidone stabilizer, we conducted a control experiment with an individual PVP solution prepared in a similar way. The concentration of the solution was 0.03 mol/L. Fig. 1(d,e) show that the PVP solution is stable under UV light, irrespective of the number of cycles.

Analysis of the dehydrogenase activity *via* MTT assay after 24 and 72 hours of incubation with tungsten oxide nanoparticles showed a dose-dependent viability decrease (Fig. 2). In particular, viability of mouse fibroblasts was significantly reduced after 24 hours of culturing with WO_{3-x} NPs (5 – 15 mg/ml). Analysis of cell viability after 72 hours of culturing also showed a significant decrease in the dehydrogenase activity for all the studied concentrations of WO_{3-x} nanoparticles (1 – 15 mg/ml). Such decrease indicates disturbances in the functioning of mitochondria. Considering the ability of WO_{3-x} NPs to generate ROS and free radicals [10], we can suggest that oxidative stress in the cell was developed.

Analysis of the proliferative activity of the cells revealed an inhibitory effect of WO_{3-x} nanoparticles (Fig. 3). Low concentrations of WO_{3-x} nanoparticles (1 and 2.5 mg/ml) did not significantly reduce the proliferative activity of the cells (Fig. 3(b)). However, even a 5 mg/ml concentration of WO_{3-x} nanoparticles led to a 50 % inhibition of proliferative activity, resulting in the change of cell confluence. Higher concentrations of WO_{3-x} nanoparticles (10 and 15 mg/ml) resulted in more than 70 % inhibition of proliferative activity (Fig. 3(c)). Upon 72 hours incubation with higher concentrations of WO_{3-x} nanoparticles, the appearance of the cells also changed significantly. After 72 hours, almost all the cells detached from the substrate, acquired a rounded shape, losing the characteristic spreading (Figure 3a).

We analyzed the number of dead cells after incubation with WO_{3-x} nanoparticles using fluorescent dyes (Syto 9/propidium iodide) (Fig. 4). This analysis did not reveal the presence of dead cells after 24 hours of cultivation with 1 to 10 mg/ml of WO_{3-x} nanoparticles. Meanwhile, higher concentration of WO_{3-x} nanoparticles (15 mg/ml) led to the appearance of dead cells. After 72 hours of incubation, 5, 10 and 15 mg/ml concentrations of WO_{3-x} nanoparticles resulted in a significant proportion of dead cells. A significant reduction in the number of the cells indicated both an inhibitory effect on the proliferation of the cell culture and their detachment from the substrate.

We carried out gene expression analysis of the effect of tungsten oxide nanoparticles on cellular components. PCR RT method was used to analyze mRNA expression of 96 genes responsible for the development of oxidative stress response (Fig. 5). The data obtained indicated that WO_{3-x} nanoparticles led to changes in the transcriptional activity of genes associated with the development and protection against oxidative stress. The action of WO_{3-x} nanoparticles was found to be dose- and time-dependent. Thus, WO_{3-x} nanoparticles (1 mg/ml) after 24 hours incubation activated transcription of the glutathione peroxidase (*GPx*) genes (*Gpx* 1 – 3, *Gpx* 5 – 7 and *Gstk1*) and some other peroxidase genes (*Epx*, *Lpo*, *Mpo*, *Rag2*, *Serp1nb1b* and *Tpo*). There was also an increase in the transcriptional activity of a few genes associated with reactive oxygen species (ROS) metabolism (*Cyba*, *Nos2*, *Nox4*, *Il22*), six genes associated with oxidative stress response (*Ercc2*, *Hspa1a*, *Krt1*, *Txn1* and *Xpa*) and one gene of the oxygen transporters group (*Ngb*). After 72 h, a significant activation of gene expression took place, but with a different pattern. Thus, in the glutathione peroxidases and peroxiredoxins (*TPx*) cluster, an increased level

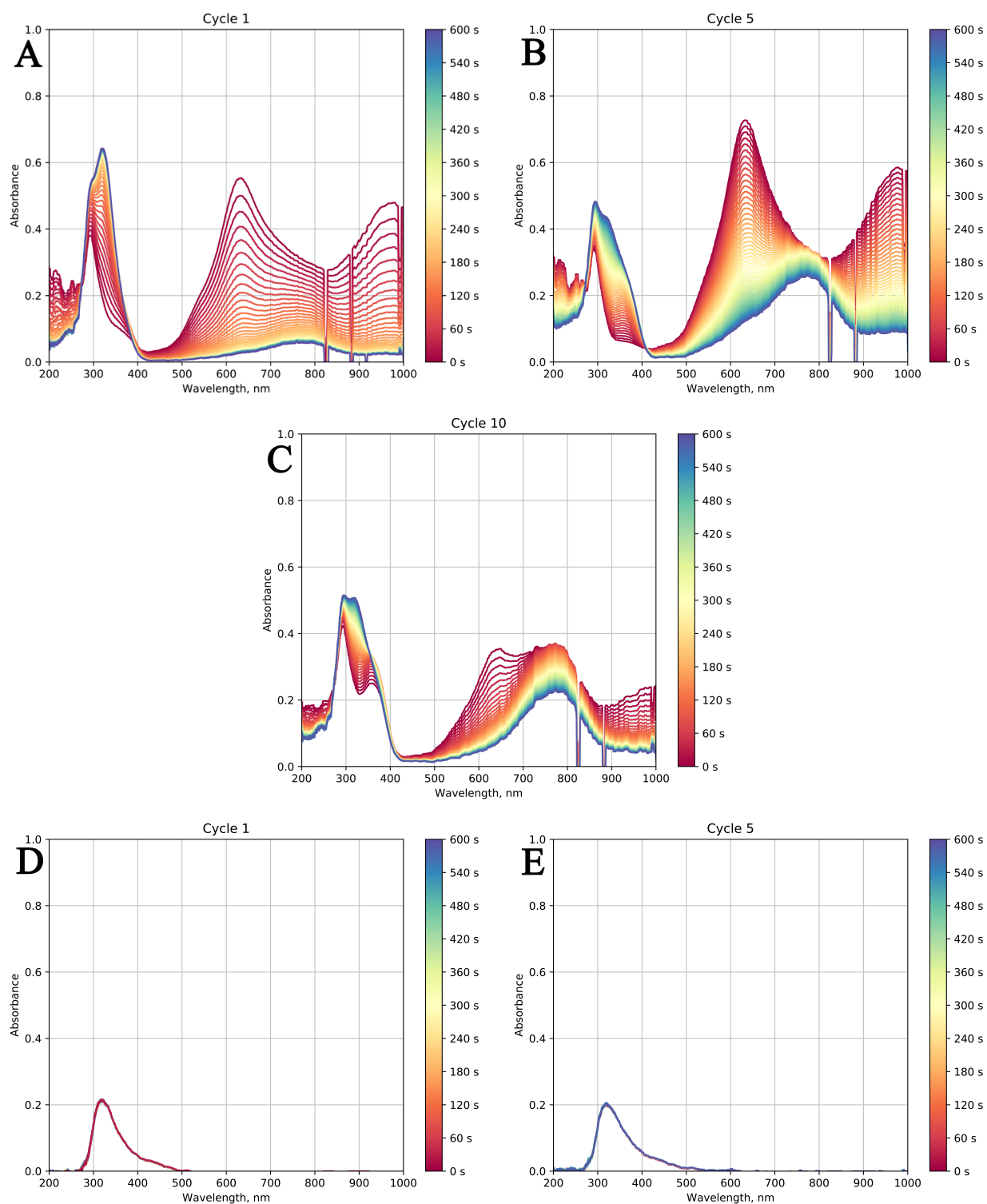


FIG. 1. Absorption spectra of the sol at the first, fifth and tenth irradiation cycle, respectively (A–C), absorption spectra of the PVP solution during the first and fifth cycle (D–E)

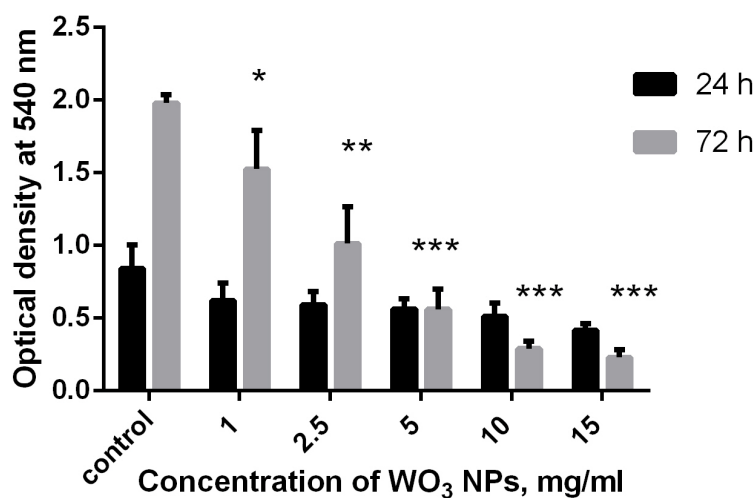


FIG. 2. Results of MTT assay 24 and 72 h after incubation of NTCT L929 cells with WO_{3-x} nanoparticles. Data are presented as mean \pm sd ($yEr\pm$), $n = 3$. * - $p \leq 0.05$, ** - $p \leq 0.001$, *** - $p \leq 0.0001$ according to Mann-Whitney U-test

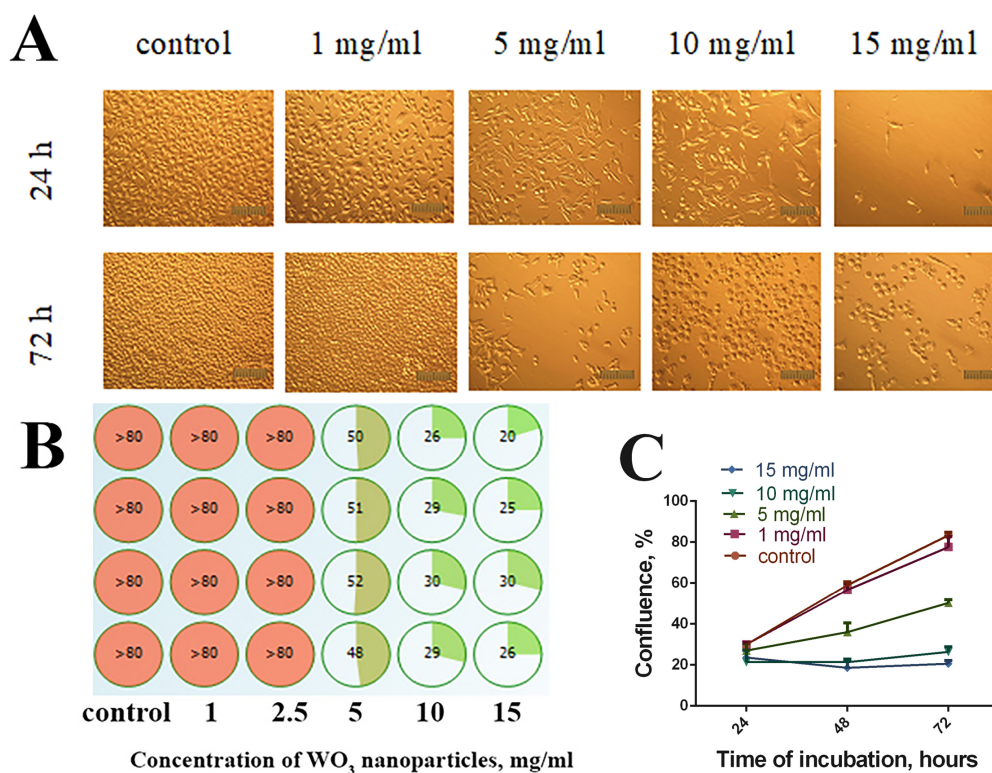


FIG. 3. Microphotographs of NCTC L929 cells after 24 and 72 h incubation with WO_{3-x} nanoparticles (1 – 15 mg/ml) (A). Confluence of NCTC L929 cells after 72 h of incubation with WO_{3-x} nanoparticles (1 – 15 mg/ml) (B). Growth curve of NCTC L929 cells after 3 day incubation (C). Cells were plated in 96 well plates and left overnight. Then WO_{3-x} nanoparticles (1 – 15 mg/ml) were added and after 24, 48 and 72 h cells confluence was analyzed

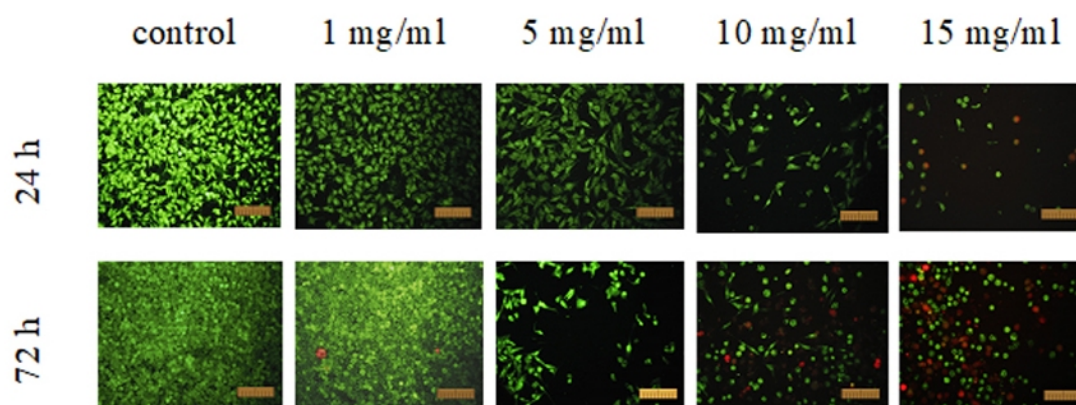


FIG. 4. Microphotographs of NCTC L929 cells after 24 and 72 h incubation with WO_{3-x} nanoparticles (1 – 15 mg/ml). Cells were plated in 96 well plates and left overnight. Then WO_{3-x} nanoparticles (1 – 15 mg/ml) were added and after 24 and 72 h cells were stained with L-7007 LIVE/DEAD kit

of transcription of only 3 genes (*Gpx2*, *Gpx3* and *Ehd2*) was recorded, and the expression level of some genes of this group was reduced compared to the control (*Gpx5*, *Gpx6* and *Gstk1*). During this period, an increase in the expression of genes of other peroxidases (*Apc*, *Cat*, *Duox1*, *Lpo*, *Ptgs2*, *Serpin1b* and *Tpo*) occurred. In contrast to the 24-hour incubation period, after 72 hours incubation, NCTCT L929 cells showed increased transcription of 2 other antioxidant genes (*Alb* and *Txnrd2*), and in the cluster of other superoxide metabolism genes 7 genes were up-regulated - *Cyba*, *Nox1*, *Noxa1*, *Recq14*, *Scd1*, *Aox1* and *Il19*.

Compared to 24 h incubation, an increase in the transcription of a larger number of genes (*Als2*, *Apoe*, *Ccl5*, *Ercc6*, *Ercc2*, *Gclc*, *Sqstm1*, *Txn1*, *Txnip*, and *Ucp3*) occurred in the oxidative stress responsive genes cluster. In the group of oxygen transporters, there was a total activation of the expression of all genes, except for *Vim*. WO_{3-x} nanoparticles at the concentration of 10 mg/ml led to an increase in the transcriptional activity of genes involved in the development of oxidative stress. Meanwhile, the transcriptional expression patterns were very similar to those recorded for 1 mg/ml concentration after 72 hours of incubation. At the same time, in some clusters, a significant decrease in the expression of some genes was observed (*Gpx2*, *Gstp1*, *Ehd2*, *Prdx1*, *Prdx2*, *Prdx3*, *Cat*, *Serpin1b*, *Gsr*, *Sod3*, *Txnrd1*, *Txnrd3*, *Noxo1*, *Scd1*, *Ucp2*, *Gclc*, *Gcl*, *Im*, *Txnrd3*, *Noxo1*, *Scd1*, *Ucp2*, *Gclc*, *Gcl*, *Im*, *Txnrd3*, *Noxo1*, *Scd1*, *Ucp2*, *Gclc*, *Gcl*, *Cygb*, *Fance*, *Vim*). After 72 hours of cell incubation with 10 mg/ml WO_{3-x} concentration, up-regulation of the maximum number of genes was observed. Thus, in peroxiredoxins group (*TPx*) and other antioxidants, all studied genes were upregulated, as well as 70 % genes in the oxidative stress responsive cluster. Despite this, expression of some genes was down-regulated (*Gpx2*, *Gpx3*, *Gpx5*, *Gpx6*, *Gstk1*, *Epx*, *Mpo*, *Rag2*, *Ncf1*, *Nos2*, *Noxo1*, *Fmo2*, *Hspala*, *Krt1* and *Ngf*). This suggests that WO_{3-x} nanoparticles have a pronounced pro-oxidant activity. Our results showed that WO_{3-x} nanoparticles are able to significantly modulate both pro- and antioxidant gene expression. Firstly, WO_{3-x} nanoparticles activated the glutathione peroxidases and peroxiredoxins after 24 h even at low concentrations (1 mg/ml). Higher concentration of WO_{3-x} nanoparticles (10 mg/ml) led to the activation of the transcriptional activity of other antioxidant protection genes and genes responsible for ROS metabolism.

4. Conclusions

PVP-stabilized tungsten oxide nanoparticles provide dose- and time-dependent inhibition of the mouse fibroblasts proliferative activity due to the induction of strong oxidative stress leading to cell death. The intermediate concentration of WO_{3-x} nanoparticles (5 mg/ml) showed significant inhibition of proliferation, while higher concentrations (10 and 15 mg/ml) resulted in the development of apoptosis and cell death. WO_{3-x} concentrations less than 2.5 mg/ml did not cause an increased cell death and did not significantly affect cell metabolism. The obtained data indicate that WO_{3-x} nanoparticles may have a potential toxic effect on mammalian cells.

Acknowledgements

This study was funded by Russian Science Foundation (project 18-73-10150).

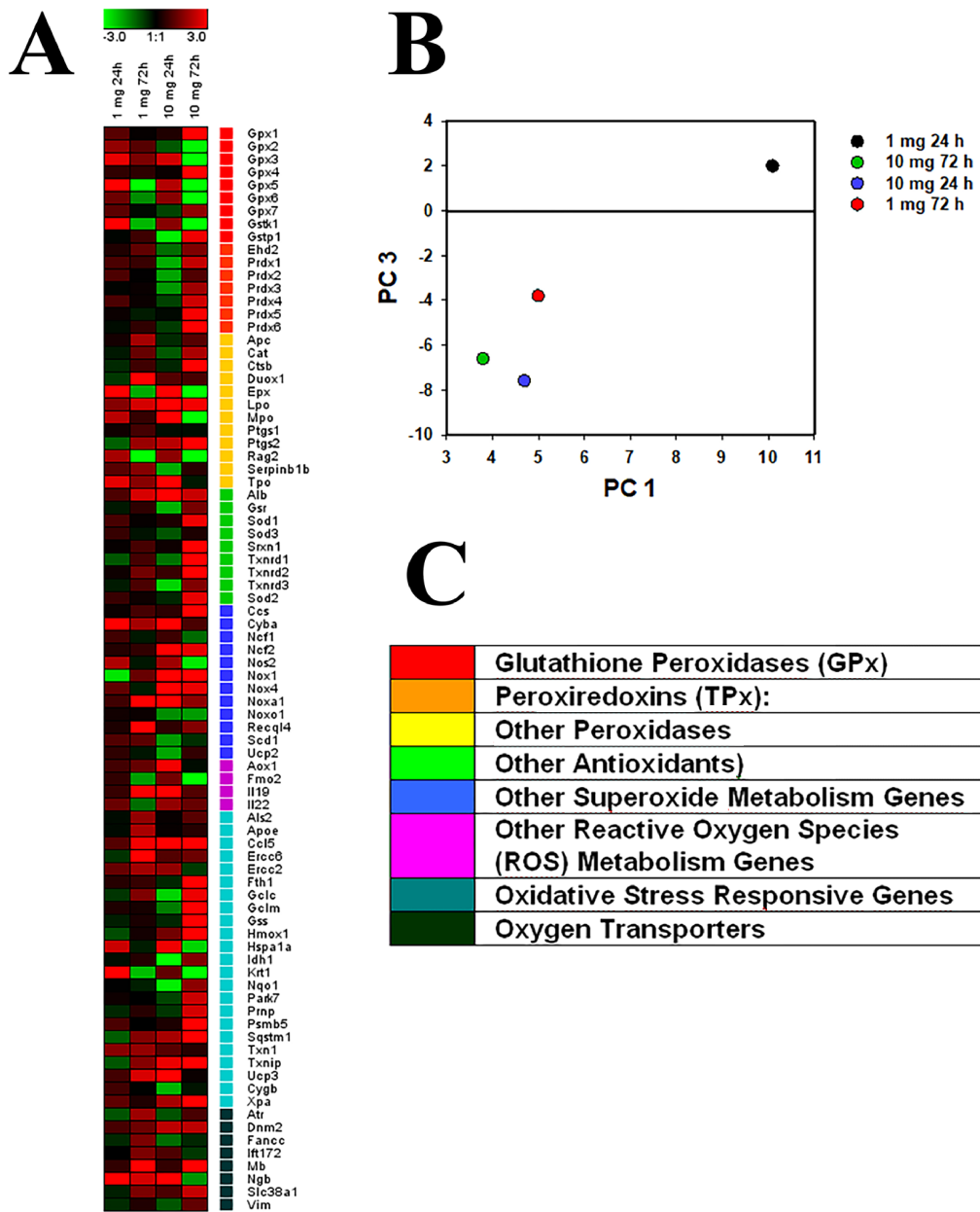


FIG. 5. Heat map of gene expression in NCTC L929 cells treated with WO_{3-x} nanoparticles (1 and 10 mg/ml) after 24 and 72 h of incubation (A). The intensity scale of the standardized expression values ranges from -3 (green: low expression) to +3 (red: high expression, with 1:1 intensity value (black) representing the control (non-treated)). Principal component analysis (PCA) of qRT-PCR data from different concentration of WO_{3-x} nanoparticles (B). Cluster groups of genes and their functionality (C)

References

- [1] Firouzi M., Poursalehi R., et al. Chitosan coated tungsten trioxide nanoparticles as a contrast agent for X-ray computed tomography. *Int. J. Biol. Macromol.*, 2017, **98**, P. 479–485.
- [2] Popov A.L., Savintseva I.V., et al. Cytotoxicity analysis of gadolinium doped cerium oxide nanoparticles on human mesenchymal stem cells. *Nanosyst. Phys. Chem. Math.*, 2018, **9** (3), P. 430–438.
- [3] Popov A.L., Shcherbakov A.B., et al. Cerium dioxide nanoparticles as third-generation enzymes (Nanozymes). *Nanosyst. Phys. Chem. Math.*, 2017, **8** (6), P. 760–781.
- [4] Popova N.R., Popov A.L., Shcherbakov A.B., Ivanov V.K. Layer-by-layer capsules as smart delivery systems of CeO₂ nanoparticle-based theranostic agents. *Nanosyst. Phys. Chem. Math.*, 2017, **8** (2), P. 282–289.
- [5] Popov A.L., Popova N.R., et al. Cerium oxide nanoparticles stimulate proliferation of primary mouse embryonic fibroblasts *in vitro*. *Mater. Sci. Eng., C*, 2016, **68**, P. 406–413.
- [6] Hosseini F., Rasuli R., Jafarian V. Immobilized WO₃ nano-particles on graphene oxide as a photo-induced antibacterial agent against UV resistant *Bacillus Pumilus*. *J. Phys. D: Appl. Phys.*, 2018, **51** (14), 145403.
- [7] Hariharan V., Radhakrishnan S., et al. Synthesis of polyethylene glycol (PEG) assisted tungsten oxide (WO₃) nanoparticles for L-dopa bio-sensing applications. *Talanta*, 2011, **85** (4), P. 2166–2174.
- [8] Deng K., Hou Z., et al. Enhanced Antitumor Efficacy by 808 nm Laser-Induced Synergistic Photothermal and Photodynamic Therapy Based on a Indocyanine-Green-Attached W₁₈O₄₉ Nanostructure. *Adv. Funct. Mater.*, 2015, **25** (47), P. 7280–7290.
- [9] Chen Z., Wang Q., et al. Ultrathin PEGylated W₁₈O₄₉ nanowires as a new 980 nm-laser-driven photothermal agent for efficient ablation of cancer cells *in vivo*. *Adv. Mater.*, 2013, **25** (14), P. 2095–2100.
- [10] Sharker S.Md., Kim S.M., et al. Functionalized biocompatible WO₃ nanoparticles for triggered and targeted *in vitro* and *in vivo* photothermal therapy. *J. Control. Release*, 2015, **217**, P. 211–220.
- [11] Zhou Z., Kong B., et al. Tungsten Oxide Nanorods: An Efficient Nanoplatform for Tumor CT Imaging and Photothermal Therapy. *Sci. Rep.*, 2014, **4**, 3653.
- [12] Liu J., Han J., et al. *In vivo* near-infrared photothermal therapy and computed tomography imaging of cancer cells using novel tungsten-based theranostic probe. *Nanoscale*, 2014, **6** (11), P. 5770–5776.
- [13] Liu P., Wang Y., et al. Ultrasmall WO_{3-x}@ γ -poly-L-glutamic Acid Nanoparticles as a Photoacoustic Imaging and Effective Photothermal-Enhanced Chemodynamic Therapy Agent for Cancer. *ACS Appl. Mater. Interfaces*, 2018, **10** (45), P. 38833–3884.
- [14] AbuMousa R.A., Baig U., et al. Photo-catalytic Killing of HeLa Cancer Cells Using Facile Synthesized Pure and Ag Loaded WO₃ Nanoparticles. *Sci. Rep.*, 2018, **8**, 15224.
- [15] Popov A., Zholobak N., et al. Photo-induced toxicity of tungsten oxide photochromic nanoparticles. *J. Photochem. Photobiol. B*, 2018, **178**, P. 395–403.